LABELLED MICROSPHERES ASSESSMENT USING 1.5T SCANNER FOR EMBOLIZATION FOLLOW UP

Hassan Jassar, François Langevin

Université de Technologie de Compiègne – Centre d'Imagerie Médicale Avancée, 60471 Compiègne, France
{hassan.jassar, Francois.langevin}@utc.fr

ABSTRACT

Controlled fibroids and tumors embolization with magnetic resonance imaging (MRI) remain challenging due to the absence of effective detection with another imaging modality. The objectives of this paper were to assess by 1.5T MRI the detectability of superparamagnetic iron oxide (*SPIO*) labelled microspheres (*LB*MSs*) with the help of three models. Four size ranges of *LB*MSs* were firstly injected into 8 *ex vivo* sheep kidneys or were secondly embedded in a hydrogel of a Petri dish as different grouping. The feasibility of *in vivo* assessment was thirdly determined in *in vitro model* according to *LB*MSs* size, coils, FOV, and sequence. *LB*MSs* appeared as black spots in MRI sheep Kidney images, different grouping of *LB*MSs* appeared as a single black spot in MRI images of Petri dishes, and a positive visualization in *in vivo* conditions. Our models demonstrate the efficiency of *LB*MSs* assessment, *in vitro* and *in vivo* conditions, with MRI according to different sizes. **Index Terms:** Magnetic resonance imaging, sequences, coils, spheres, tumors.

INTRODUCTION

Embolization is the process of cutting off the blood flow to a tumor, or in essence, starving it of oxygen and the nutriments it needs to exist, grows and metastasize [1].

Controlled embolization with MRI is an important innovation for fibroids and solid tumor treatment. Currently, angiography only allows the visualisation of blood flow inside the vessels, but particles used in the embolization procedure remain invisible and induced *cm* range errors [1]. As a result, it is still a challenge to verify if these particles are located at the right places inside vessels.

Magnetic resonance (MR) detectable *LB*MSs*, with super-*SPIO*, would allow a better control of emboli introduction after embolization. Moreover, detectable particles will help doctors evaluate the success of an embolization procedure by appreciating the particles' location inside or outside the tumor, homogeneous or heterogeneous distribution in/around it and their optimal density per tumor volume.

The purpose of this works is to evaluate with MRI the visualization of *LB*MSs* according to their MR signal, contrast, appearance, shape, size and number. In addition, MR sequence parameters and coil have studied whether they have any affect on MR *LB*MSs* detectability. Three models—one *ex vivo* and two *in vitro*—were developed for this purpose. Renal sheep vasculature was used as an *ex vivo* model for embolization with either four ranges of Embosphere microspheres (*EMs*) or *LB*MSs* (100-300, 300-500, 500-700 and 700-900 µm). With MR imaging, this model provides a visualisation of the different renal regions covered by the different *LB*MSs* sizes, as well as their distribution inside the renal arterial vasculature. The first *in vitro* model evaluated the way in which *LB*MSs* appear in MRI images, based on their size and grouping in a Petri dish. The second in vitro model was designed to predict the *in vivo* feasibility to detect *LB*MSs* used as a vascular fibroid emboli.

MATERIALS AND METHODS

Trisacryl Microspheres Labelled by SPIO:

Hydrophilic Trisacryl co-polymer microspheres (MSs) coated with porcine gelatine was loaded with homogenously distributed *SPIO* (Dextran-Magnetite) particles, in order to exhibit a MR signal different from that of non loaded MSs and that of the biological medium [2]. Non-resorbable Trisacryl MSs, which have a spherical shape, allow accurate grading and optimal geometric distal vessel occlusion [3]. They are precisely calibrated, micro-porous beads, inert, translucent and they have demonstrated biocompatibility [4]. The suppleness of these MSs prevents their aggregation of catheters [5].

Two groups of Trisacryl MSs were used in the study. Each group contained four granulometric ranges: 100-300, 300-500, 500-700, and 700-900 µm. One of the groups included calibrated embosphere microsphere (*EM)*–Embosphere-Biosphere Medical SA–used as a control; the other contained a prototype of calibrated MS loaded with a contrast agent (Dextran-Magnetite) to make MSs MR detectable.

Renal Embolization Protocol

Renal vessels are represented as a network of arteries and veins. Hierarchy in vessels, diameters and blood flow makes the kidney a suitable model for embolization procedures. The particles' specific gravity, small size, and smooth, round surface allow these microspheres to reach more distally, to vessels with diameter approximating their own. This produces a more complete and permanent occlusion [6].

Four sheep were selected by a radiologist according to their weight, and each received one of the four granulometric ranges of

*LB*MSs* in one kidney and a comparable size of EMs in the other. Embolization was performed in the Center of Research in Interventional Radiology (CR2I) and the French National Institute for Agriculter Research (INRA, Joy-en-Josas, France). The following day, the animals were sacrificed. Each pair of kidneys was removed and conserved in a container with a 10% formaldehyde solution. The containers were labelled according to the size of the MS used in the embolization (100-300, 300-500, 500-700 and 700-900 µm, respectively).

Hardware

All imaging was performed using a superconducting 1.5 Tesla MR system (General Electric Medical System-EXCITE™ 11.0) in the CIMA laboratory at the Compiegne University of Technology (UTC-France). Four-element phased array coils were used as radiofrequency receivers (MACHNET-PACC-GS15 and CARDIAC). These coils were chosen for their favorable signal-to-noise ratio and their usefulness in determining the feasibility of *in vivo LB*MS* detection with MRI.

MR Sequences and Parameters

Ex vivo imaging

The imaging of each renal container was performed six weeks after the sheep were sacrificed. Three-dimensional Fourier transform spoiled-gradient echo (3DFT SPGR) and two-dimensional Fourier transform Fast spin echo (2DFT FSE-XL) sequences were implemented separately for exploring the embolized kidney.

3DFT SPGR is *T_1-weighted* (T_1w) and 2DFT FSE is *T_2-weighted* (T_2w). Both weightings were used to determine which one would be the most suitable for the detection of *LB*MSs*. All images were acquired in the coronal and sagittal plane, with a field of view (FOV) of 100 × 100 mm. The MACHNET coil was centered on the different renal containers in order to obtain maximum signal intensity.

The *T_1w* 3DFT SPGR sequence was acquired using a matrix size of 256 × 256, a repetition time (TR) of 30 ms and an echo time (TE) of 9 ms. A total of 28 slices with 1 mm thickness were acquired for an acquisition time of 4.09 minutes.

Sagittal *T_2w* 2DFT FSE-XL images was acquired using a matrix size of 256 × 256, a TR of 3000 ms and a TE of 120 msec. The voxel size was 0.4 × 0.4 × 2.0 mm^3. The number of slices was 13 with no intersection gap. The number of excitations (Nex) was 3 and the echo train length (ETL) was 16. The total acquisition time for this sequence was 2.30 minutes.

In vitro imaging

3DFT SPGR, 2DFT FSE and 3DFT Fiesta sequences were implemented for in vitro Petri dish imaging. 3DFT Fiesta is T_2/T_1-weighted (T_2/T_1w).

The 3DFT-Fiesta sequence was acquired using a short TR value (7 msec), a minimum TE (3 msec) and an axial image with 52 slices of 2 mm thickness. Two FOVs were used: 100 × 100 mm or 140 × 140 mm, depending on the experiences explained in following paragraphs. The flip angle was 45°, the matrix size was 256 × 256 and the Nex was 0.5. Slice zero fill processing (Zip), which interpolates new slice locations in a 3D volume, was used to increase through plane resolution and to reduce partial volume artefact. The total acquisition time for this sequence was 31''.

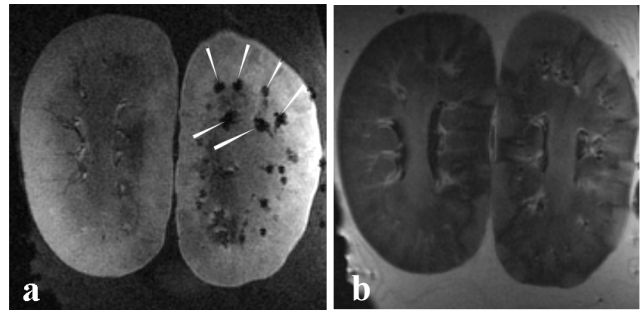

Figure 1 : *a) T1 w ex vivo images of sheep kidneys. Black spots appear in the medulla zone of the left kidney due to LB*MS (white arrows) with a 700-900 µm of size, whereas EMs are not seen in the left kidney. b) T2 w image. LB*MSs and EMs don't appear on right and left renal image.*

Petri Dish Preparation and Imaging

The first *in vitro* study was designed to determine the difference between the apparent diameter in MRI and the real diameter of the MSs, as well as to check the individualization of each MS in a cluster. We created four matrices of consisting of different *LB*MS* configurations (singlet, doublet, triplet and cluster) in each quarter of a Petri dish of diameter ≈ 85 mm. Different sizes of MSs (100-300, 300-500, 500-700 and 700-900 µm, respectively) were used in each quarter. The preparation of the Petri dish, was started with a layer of a transparent gel (Biomerieux, ref41466) in order to support each matrix of *LB*MS*. To form the matrix, a few ml of *LB*MS* suspended in a physiological serum was filled in a syringe and then dropped on the gel layer under microscope control (Ellix® 5.2.2). All *LB*MS* matrices were then covered by a new gel layer. As a result, the matrices of *LB*MS* remained fixed between the two protective layers of gel. This preparation was performed in the CR2I laboratory, where microscopic images of the Petri dish were taken. MRI acquisition of the Petri dish was done in the CIMA laboratory, using *T1w* and *T2w* sequences previously described for the *ex vivo* model, but with fewer slices and a shorter acquisition time.

Petri Dish Imaging with In-vivo Conditions

The purpose of this study was to verify the feasibility of *LB*MS* detection with MRI in *in vivo* conditions. This study used one Petri dish with diameter ≈ 50 mm was prepared similarly to the dishes used in the first *in vitro* study. (500-700µm) *LB*MS* range, which is preferred to achieve fibroid devascularisation [7], was embedded in a hydrogel of a Petri dish as different distributions.To simulate *in vivo* conditions, the Petri dish was placed in the centre of a cylindrical bucket (diameter ≈ 16 cm) in order to provide distance between the coil and the microspheres. A CARDIAC coil was used to obtain larger FOV (140 x 140 mm), similar in size to an *in vivo* application. These results were then compared to images obtained by placing the MACHNET coil directly on the Petri dish (FOV 100 x 100 mm). The T_2/T_1w 3DFT Fiesta sequence previously described was followed for both approaches.

Image Analysis

Quantitative analysis of all MRI images was done in the CIMA laboratory using an Advantage Windows (4.1- GE) workstation.

To assess the detection and distribution homogeneity of MSs

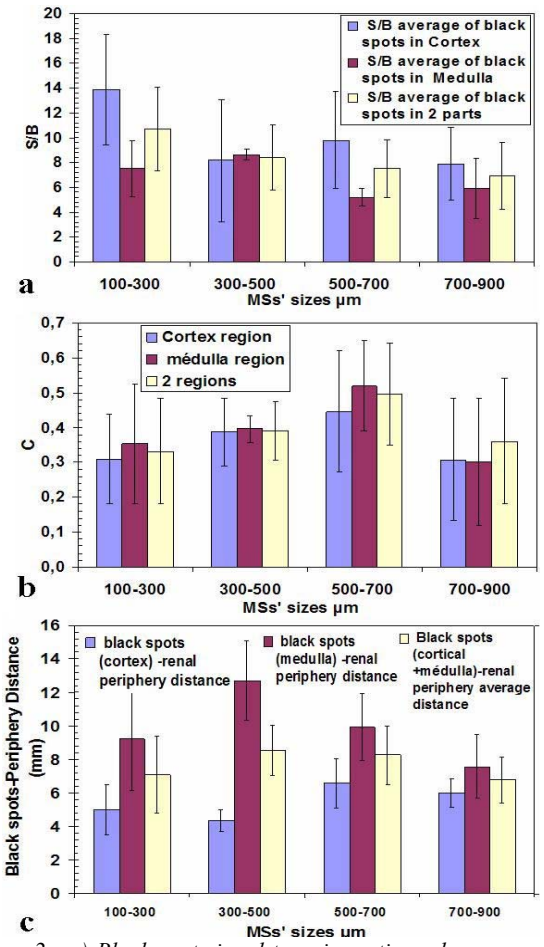

Figure 3 : *a) Black spot signal to noise ratio and average values for all MS's sizes presented in renal cortex and medulla. b) Black spot-parenchyma contrast and average values for all MS's sizes presented in renal cortex and medulla. c) Black spot-renal periphery distance and average values for all MS's sizes presented in renal cortex and medulla.*

in the *ex vivo* study, the SNR, contrast and distances of the *LB*MS*, which appeared as black spots in T_1w-renal images, were measured. Signal intensities (SIs) were determined with a standard region-of-interest (ROI) measurement in the cortex and medulla regions of the kidneys. Contrast between the black spots and the renal parenchyma was calculated as $(SI_{Parenchyma} - SI_{Spot})/(SI_{Parenchyma})$ to assess the appearance of *LB*MS* in the medium. Distance between the black spots and the renal periphery was determined for each size of MS. As a result, the depth reached by the MSs inside the renal vessels evaluates their distribution since the size of the MSs corresponds to the diameter of the vessels.

The Petri dish study, in first *in vitro* model, compared the dimensions of the *LB*MS* in the T_1w and the microscopic images. In the T_1w Petri dish images, the dimensions of the black spots (diameter for circular spots, length and width for irregularly shaped spots) were determined. These values were compared to the dimensions measured in the microscopic images using the graphical software available on the PC at CR2I. Excel software was used to calculate the correlation between the microscopic and T_1w images.

In the *in vivo* simulation study, the feasibility of *LB*MS*

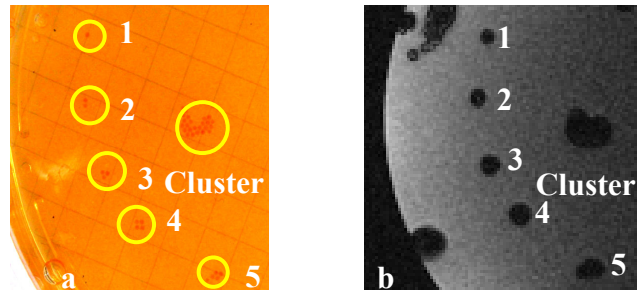

Figure 2 : *Microscopic and MR images of a quadrant of a Petri dish corresponding to a one size of LB*MS (500-700 µm). a) Microscopic image, a matrix of LB*MS grouped as a singlet, doublet, triplet and cluster (yellow round). b) T1 w image of a quadrant of the Petri dish. Black spots are in correspondence to different LB*MS configurations.*

detection with MRI was estimated by comparing the T_2/T_1w images obtained with the MACHNET and CARDIAC coils.

RESULTS AND DISCUSSION

In the present paper we have proposed three models that make it possible to 1) estimate the detection and the distribution of the *LB*MS* through an *Ex vivo* analysis, 2) evaluate the appearance and the magnification of the *LB*MS* obtained in the MR images (*in vitro* analysis) and 3) verify the possibility of MR detection of *LB*MS* via *in vivo* approach.

Ex vivo

Fig. 1 displays the images acquired from the kidneys of the sheep used in this study. The T_1w images (3DFT SPGR) represent the *LB*MS* as black spots (Fig.1a-right), whereas in T_2w images (2DFT FSE) the *LB*MS* remain invisible (Fig.1b-right). However, control MSs do not appear in either T_1w or T_2w images (Fig.1a and b-left). This demonstrates that the 3DFT SPGR sequence is suitable for MRI of the *LB*MS* with *SPIO*.

The use of the 3DFT acquisition gives a significant advantage for clinical applications. As it uses very thin slices with no slice gaps (contiguous slices), it ensures that no MSs are missed during the scan. Slices can also be reformatted on a workstation to produce images in any orientation. Furthermore, 3DFT scanning is important when a high resolution is required.

The effect of the *LB*MS* size on the SNR measurement in the cortex and medulla regions shows a decrease in the SNR value as the MS size increases (Fig. 2a). However, the contrast measurement in the two regions shows an increase in the contrast value between the black spots and the parenchyma as the MS size increases (Fig. 2b). As a result, in T_1-weighted images the microspheres appear as dark spots.

The result of the distance measured between the black spots and the renal periphery shows a decrease in the distance value as the MS size increases (Fig. 2c). This is a result of a decline in vessel diameter that is widespread at the periphery.

In vitro

The difference between the apparent and real diameters of the MSs (shown in the MRI and microscopic images, respectively) as well as the individualization of each microsphere in a multiple MSs, is shown in (Fig. 3a and b). For the individual MSs of all sizes, the shape of the black spots is essentially circular. However

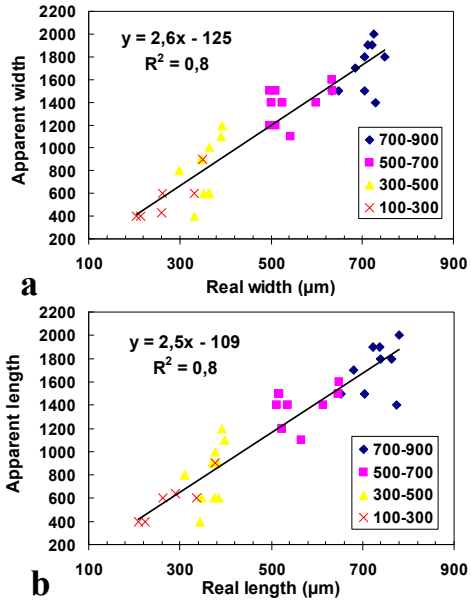

Figure 5 : *Correlation between the apparent and real width (a) and length (b) of singlet LB*MS for all sizes.*

MS grouping	Magnification		R^2	
	Length	Width	Length	Width
Doublet MS	1.3	1.6	0.7	0.5
Triplet MS	1.4	1.6	0.8	0.7

Table 1 : *Length and width Values of Black spots obtained from MSs in Doublet and Triplet Grouping. The relationship between the apparent and real dimension of MS in two groups is depicted by R^2.*

in the case of multiple MSs, each cluster of MSs appears as a single ellipse in the MRI images. Since one black spot was always obtained regardless of the number of MSs in each group, this implies the impossibility of discriminating in T_1w images the number of *LB*MS* in a group.

MR magnification of single *LB*MS* diameters was 2.5 for all MS sizes (Fig. 4a, b). The magnification factor decreases in the case of doublet, triplet and cluster MSs, as shown in Table 1.

The correlation coefficient (R^2) between the real and apparent dimension of *LB*MS* equals (0.5 - 0.8). These values exhibit a significant linear relationship for single and multiple MSs. This linearity in the magnification is attributed to the effect of the superparamagnetic particles on the surrounding environment by disturbing the local magnetic field that the protons experience [8].

From this study, the factor of magnification determined according to the size and number of MSs provides an important guideline for spatial resolution optimization. This optimization avoids the partial volume effects by matching the size of the pixel/voxel to the real size of the MS. As a consequence, pixel size can be calculated by multiplying the magnified factor to the real size of MS.

In-vivo simulation

The results of the patient simulation for the MRI *LB*MS* assessment using a small and large coil are shown in Fig. 5. The

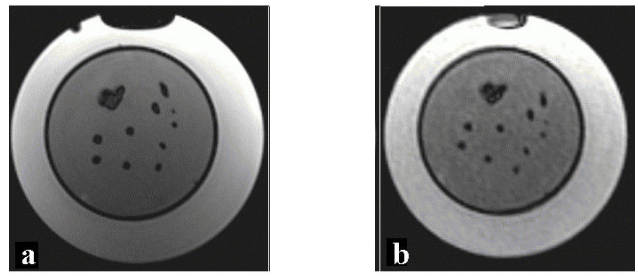

Figure 4 : *Ultra fast imaging of Petri dishes which contain LB*MS (500-700 µm) in: singlet, doublet, triplet and cluster configuration. a) MR image is obtained by Kneepa coil according to a 10 cm of Field of view and 31 sec of acquisition time. Kneepa coil is placed directly to the Petri dish. b) MR image is obtained by cardiac coil according to a 14 cm of Field of view and 31 sec of acquisition time. Cardiac coil is placed distantly from the Petri dish.*

image obtained by the CARDIAC coil (FOV 14 cm) in Fig. 5b represents the black spots clearly, similar to the result in the image obtained by the MACHNET coil (FOV 10 cm) in Fig. 5a. This proves the feasibility of *in vivo* detection of the *LB*MS* with MRI. The 3DFT Fiesta sequence permits an increase in signal intensity and a reduction in acquisition time. This reduction can minimize the motion artefact (respiratory).

CONCLUSION

*LB*MS* can be detected with MRI to provide an accurate embolization of fibroids and solid tumors. Spatial resolution is optimized according to the magnification factor of *LB*MS* in MR images. *LB*MS* detection in *in vivo* conditions with ultra fast MR sequence is acceptable and will be useful in human application.

REFERENCES

[1] Laurent A et al. Partition of calibrated tris-acryl gelatin microspheres in the arterial vasculature of embolized nasopharyngeal angiofibromas and paragangliomas. J Vasc Interv Radiol 16:507-513, 2005.

[2] Laurent A, Labarre D. Hydrophilic polymer biomaterial having a specific magnetic resonance imaging signal and process for the preparation of said biomaterial. *US2003077225,* 24-04-2003.

[3] Domas L et al. Morphological analysis and shape index of embolization particles. *Innov Tech Biol Med*, 14: 436-448, 1993. (in French)

[4] Laurent A et al. Trisacryl gelatine microspheres for therapeutic embolization, I: development and in vitro evaluation. *AJNR Am J Neuroradiol*, 17: 533-540, 1996.

[5] Beaujeux R et al. Trisacryl Gelatin Microspheres for Therapeutic Embolization, II: Preliminary Clinical Evaluation in Tumors and Arteriovenous Malformations. *AJNR Am J Neuroradiol* 17:541–548, March 1996.

[6] Dion J E et al. Dextran microsphere embolization: Experimental and clinical experience with radiologic-pathologic correlation. *Radiology*, 160:717-721, 1986.

[7] Pelage J. P et al. Limited Uterine Artery Embolization with Trisacryl Gelatin Microspheres for uterin Fibroids. J Vasc Interv Radiol 14:15–20, 2003.

[8] Boxerman et al. 1995. Kennan et al. Quantitative MRI of brain, page 370, 1994.